

Research Article

A Strange Double-Deck Butterfly Chaotic Attractor from a Permanent Magnet Synchronous Motor with Smooth Air Gap: Numerical Analysis and Experimental Observation

Zhonglin Wang,¹ Shijian Cang,² Zenghui Wang,³ Wei Xue,⁴ and Zengqiang Chen⁵

¹ Department of Physics and Electronics Science, Binzhou University, Binzhou 256604, China

² Department of Industry Design, Tianjin University of Science and Technology, Tianjin 300457, China

³ Department of Electrical and Mining Engineering, University of South Africa, Florida 1710, South Africa

⁴ Department of Automation, Tianjin University of Science and Technology, Tianjin 300457, China

⁵ Department of Automation, Nankai University, Tianjin 300071, China

Correspondence should be addressed to Shijian Cang; sj.cang@gmail.com

Received 30 April 2014; Accepted 1 July 2014; Published 17 July 2014

Academic Editor: Roberto Barrio

Copyright © 2014 Zhonglin Wang et al. This is an open access article distributed under the Creative Commons Attribution License, which permits unrestricted use, distribution, and reproduction in any medium, provided the original work is properly cited.

A permanent magnet synchronous motor (PMSM) model with smooth air gap and an exogenous periodic input is introduced and analyzed in this paper. With a simple mathematical transformation, a new nonautonomous Lorenz-like system is derived from this PMSM model, and this new three-dimensional system can display the complicated dynamics such as the chaotic attractor and the multiperiodic orbits by adjusting the frequency and amplitude of the exogenous periodic inputs. Moreover, this new system shows a double-deck chaotic attractor that is completely different from the four-wing chaotic attractors on topological structures, although the phase portrait shapes of the new attractor and the four-wing chaotic attractors are similar. The exotic phenomenon has been well demonstrated and investigated by numerical simulations, bifurcation analysis, and electronic circuit implementation.

1. Introduction

Due to simple structure, low manufacturing cost, and high performance [1], permanent magnet synchronous motors (PMSMs) are widely used in modern direct drive motor systems [2, 3], power conversion [4, 5], computer disk drives [6, 7], and domestic applications [8, 9]. Compared with DC motors and induction motors, PMSMs have the advantages of high speed operational capability, precise torque control, high torque to current ratio, high power to weight ratio, high efficiency, and high robustness to exogenous disturbances [10]. Recently, the studies about the secure and stable operation of PMSMs, which is an essential requirement of industrial automation manufacturing, have attracted more and more attentions. Some research results showed that PMSMs are chaotic when system parameters change within certain ranges [11–13]. The chaotic behavior in PMSMs, which appears mainly as intermittent ripples of torque,

low-frequency oscillations of rotational speed of motor, can extremely destroy the stability of the motor and even induce drive system collapse.

Because the mathematical model for a PMSM is a typical nonlinear system and it cannot be analyzed based on the linear theory, the modern nonlinear theory such as bifurcation and chaos, which has been widely used to study the stability of nonlinear systems, can be used to study the permanent magnet machines. Li et al. deeply analyzed the bifurcation and chaos in PMSM with smooth air gap in various cases that stator voltages on rotating frame and external load torque are equal to zero in whole or part [11]. However, their studies about the nonzero external inputs of PMSM are only limited to DC power supply, without considering AC power supply. For the PMSM with nonsmooth air gap, Jing et al. studied the complex dynamics including the stability, the pitchfork, and Hopf bifurcations using the bifurcation theory and the center manifold [14]. In order to avoid chaos in PMSM, Choi gave

an adaptive control scheme for the permanent magnets based on the bifurcation analysis [15, 16]. Therefore, the above research results [11, 14–16] show that the permanent magnet machines can experience chaotic oscillations at some situations.

Because the chaotic dynamical behavior has been widely observed in practice, how to apply chaos to the engineering practice and generate strange chaotic attractors with complex topological structure by a simple dynamical system has become the focus in the field of nonlinear dynamics recently. Moreover, sometimes it is necessary to avoid the chaotic dynamics in some systems. Hence, it would be useful to investigate the dynamical behavior of PMSM and find out whether there are strange attractors. In this paper, the focuses of this study are as follows:

- (1) investigating the dynamical behavior of a PMSM model with smooth air gap with external periodic excitation to the q -axes stator on rotating frame, which has not been carefully studied;
- (2) analyzing the bifurcation and chaos of the PMSM model by phase portrait, Poincare map, Lyapunov exponents, and bifurcation diagram, which are important tools to find strange double-deck butterfly chaotic attractors and multiperiodic orbits and analyze the dynamical behavior of the PMSM model;
- (3) analyzing the power spectra of the PMSM model since the power spectrum analysis is an effective tool to explore the frequency components of state variable;
- (4) besides, validating the findings by the simulations and experimental circuits.

This paper is organized as follows. In Section 2, the mathematical model for a PMSM with external excitations is proposed. Section 3 focuses on the bifurcation and chaos in the nonautonomous PMSM system by the methods of phase portrait, Poincare map, Lyapunov exponents, bifurcation diagram, and power spectrum. In Section 4, an experimental circuit is implemented to verify the obtained numerical results. Finally, we draw the conclusions.

2. The Mathematical Model

The d - q machine model for a permanent magnet synchronous motor (PMSM) in the rotor rotating reference frame [11, 17] is characterized by

$$\begin{aligned} \frac{di_d}{dt} &= \frac{1}{L_d} (-Ri_d + L_q\omega i_q + v_d) \\ \frac{di_q}{dt} &= \frac{1}{L_q} (-Ri_q - L_d i_d \omega - \psi_r \omega + v_q) \\ \frac{d\omega}{dt} &= \frac{1}{J} [n\psi_r i_q + (L_d - L_q) i_d i_q - B\omega - T_L], \end{aligned} \quad (1)$$

where i_d , i_q , and ω are the state variables of the nonlinear dynamical system (1). The state variables i_d , i_q , and ω and

system parameters L_d , L_q , R , J , B , T_L , n , and ψ_r represent the physical meanings, respectively, as follows:

- i_d, i_q : d - and q -axes stator currents on rotating frame;
- v_d, v_q : d - and q -axes stator voltages on rotating frame;
- L_d, L_q : d - and q -axes stator self-inductances;
- ω : rotor speed at electrical angle;
- R : stator per-phase resistance;
- J : polar moment of inertia;
- B : viscous damping coefficient;
- T_L : external load torque;
- n : number of pole-pairs;
- ψ_r : permanent magnetic flux.

If $L_d = L_q = L$, the system (1) is the model of smooth air-gap synchronous machines. Applying a time-scaling transformation $t = \tau \tilde{t}$, where parameter $\tau = L/R$ is a scaling factor, and further letting

$$\tilde{i}_d = \tau \frac{n\psi_r}{B} i_d, \quad \tilde{i}_q = \tau \frac{n\psi_r}{B} i_q, \quad \tilde{\omega} = \tau \omega, \quad (2)$$

the system (1) can be rewritten as

$$\begin{aligned} \frac{d\tilde{i}_d}{d\tilde{t}} &= -\tilde{i}_d + \tilde{i}_q \tilde{\omega} + \tilde{v}_d \\ \frac{d\tilde{i}_q}{d\tilde{t}} &= -\tilde{i}_q + \gamma \tilde{\omega} - \tilde{i}_d \tilde{\omega} + \tilde{v}_q \\ \frac{d\tilde{\omega}}{d\tilde{t}} &= a(\tilde{i}_q - \tilde{\omega}) - \tilde{T}_L. \end{aligned} \quad (3)$$

Here the updated parameters are

$$\begin{aligned} \gamma &= -\tau \frac{n\psi_r^2}{BL}, \quad a = \frac{\tau B}{J}, \quad \tilde{v}_q = \tau \frac{n\psi_r}{BR} v_q, \\ \tilde{v}_d &= \tau \frac{n\psi_r}{BR} v_d, \quad \tilde{T}_L = \frac{\tau^2 T_L}{J}. \end{aligned} \quad (4)$$

Let $x = \tilde{\omega}$, $y = \tilde{i}_q$, and $z = \tilde{i}_d$; one obtains that

$$\begin{aligned} \dot{x} &= a(y - x) - \tilde{T}_L \\ \dot{y} &= \gamma x - y - xz + \tilde{v}_q \\ \dot{z} &= -z + xy + \tilde{v}_d. \end{aligned} \quad (5)$$

If $\tilde{T}_L = \tilde{v}_q = \tilde{v}_d = 0$, the system (5) evolves into the famous Lorenz system with the parameter $\rho = 1$, whose dynamical behavior has been deeply explored [18, 19]. For the system (5) with $\tilde{v}_q \neq 0$, there are two main cases: $\tilde{T}_L = \tilde{v}_d \neq 0$ and $\tilde{T}_L = \tilde{v}_d = 0$. According to the numerical simulations and experimental investigations, it was found that the dynamics of the system (5) with $\tilde{v}_q \neq 0$ and $\tilde{T}_L = \tilde{v}_d \neq 0$ is similar to that of the system (5) with $\tilde{v}_q \neq 0$ and $\tilde{T}_L = \tilde{v}_d = 0$. For the ease of analysis, this paper will only focus on the case with $\tilde{v}_q \neq 0$ and $\tilde{T}_L = \tilde{v}_d = 0$, and a new type of double-deck butterfly chaotic attractor is obtained by adjusting the control signal \tilde{v}_q , which has not been found in the existing literatures.

3. Bifurcation and Chaos Analysis of the PMSM Model

To ensure that the system (5) can be realized by electrical circuits, the variation of state variables x , y , and z of the system (5) must be limited into a proper range by the method of linear transformation and the linear transformation $(x, y, z) \rightarrow (10x, 10y, 100z)$ can be used without changing the properties of the original system. Then, the system (5) can be changed to

$$\begin{aligned} \dot{x} &= a(y - x) \\ \dot{y} &= \gamma x - y - 100xz + 0.1\bar{v}_q \\ \dot{z} &= -z + xy, \end{aligned} \tag{6}$$

where $\bar{v}_q = A \sin(\omega t)$. A and ω denote the amplitude and angular frequency of the driving signal \bar{v}_q , respectively. To analyze the system (6), there are many methods such as Lyapunov exponent spectrum [20], bifurcation diagram, phase portrait, and power spectrum, and they can be used to analyze the dynamics of nonlinear systems. The fourth-order Runge-Kutta method is used to solve the system (6) in MATLAB.

3.1. Phase Portraits and Poincare Sections. Considering the system (6) with $\bar{v}_q = A \sin(\omega t)$, we set $a = 10$ and $\gamma = 100$, respectively. Varying parameters A and ω , the dynamics of the system (6) is to be explored.

When the amplitude A and the angular frequency ω of the driving signal \bar{v}_q are not equal to zero, the system (6) is a nonautonomous three-dimensional system. By adjusting parameters A and ω , a new chaotic attractor, which was not found in the existing dynamical systems, occurs when $A = 0.2$ and $\omega = 0.6$, and meanwhile, uncommon multiperiodic orbits are observed when $A = 1$ and $\omega = 0.6$.

Case 1 ($A = 0.2$ and $\omega = 0.6$). When $A = 0.2$ and $\omega = 0.6$, the system is chaotic, but the new chaotic attractor is different from the famous attractor of the Lorenz-family systems [21] and is different from any other attractors contained in the known nonlinear dynamical system. Currently, four-wing chaotic attractors have been investigated by many researchers since the four-wing chaotic attractor shows complicated dynamics. From the shape of attractor shown in Figure 2, it can be seen that the new attractor is similar to four-wing chaotic attractor [22, 23], but the topologies are completely different between the new attractor and the known four-wing chaotic attractors since the new attractor contains two double-wing chaotic attractors, and we call this new chaotic attractor “double-deck butterfly chaotic attractor.” To check whether the system (6) is really chaotic when $A = 0.2$ and $\omega = 0.6$, we calculated the Lyapunov exponents of the system (6) via the Jacobian method and obtained the Lyapunov exponents (0.042, 0, -0.341, -11.701). Owing to the system (6) being a three-dimensional nonautonomous system, the calculating results show four exponents, among which one is greater than zero, so the system (6) is chaotic.

From Figures 1(a)–1(d), it is very clear that the new chaotic attractor is constructed by double-deck butterfly chaotic attractor, which is different from the common four-wing chaotic attractors. The projections of phase portrait on x - y , x - z , and y - z plane are shown in Figures 1(a)–1(c) and the 3D shape is in Figure 1(d), respectively.

There is another method to describe the dynamical behavior of the system (6), that is, Poincare map. Via Poincare sections, we can understand the motion of phase trajectories. Generally, the Poincare maps present several points that mean that the dynamics is periodic orbits, and countless points that form a closed curve mean that the dynamics is quasiperiodic orbits, and countless points that are self-similarly distributed at a specific region and cannot form one or more closed curves mean that the dynamics is chaotic.

On Case 1, the corresponding Poincare maps of the system (6) projected on different planes are exhibited in Figures 2(a)–2(c). Since the system (6) is chaotic, the distinct points on the Poincare sections cannot form one or more closed curves.

Case 2 ($A = 1$ and $\omega = 0.6$). When $A = 1$ and $\omega = 0.6$, a multiperiodic orbit can be found, as shown in Figures 3(a)–3(c). It can be seen from Figure 3 that the type of multiperiodic orbit has the feature of helix which is rare and different from that of periodic orbits in the known dynamical systems.

3.2. Analysis of Lyapunov Spectra and Bifurcation Diagrams. The observations in Section 3.1 are several cases under different parameters. In order to deeply explore the dynamics of the system (6) in a fixed parameter range, it is necessary to investigate the system (6) using Lyapunov spectra and bifurcation diagrams. For a nonlinear dynamical system, the largest Lyapunov exponent can denote dynamical behavior. The largest Lyapunov exponent is expressed by λ_{\max} , and then $\lambda_{\max} > 0$, $= 0$ and < 0 represent the dynamics of the system to be chaos, periodic orbit, and convergence, respectively.

For $\bar{v}_q = A \sin(\omega t)$, we set that the amplitude A is in $[0, 0.6]$ and the angle frequency ω is in $[0.4, 1]$, respectively. Fixing $A = 0.2$ and changing the angle frequency ω , the dynamical behavior of the system (6) can be shown in Figure 4. Similarly, fixing $\omega = 0.6$ and adjusting the amplitude A , the dynamical behavior of the system (6) is exhibited in Figure 5. Here, Figures 4(a) and 5(a) are the bifurcation diagrams of the state variable x for increasing ω and A , respectively. The corresponding largest exponent spectra are shown in Figures 4(b) and 5(b). From Figures 4 and 5, we can investigate the dynamics of the system (6) along with A and ω , respectively.

Further, it is necessary to characterize the dynamical behavior of the system (6) if parameters A and ω simultaneously change. Therefore, we give a two-dimensional dynamics distribution shown in Figure 6 along with the change of A in $[0, 0.6]$ and ω in $[0.4, 1]$, where the dark-cyan region denotes chaotic motion and the magenta region represents periodic motion.

3.3. Power Spectra Analysis. The different dynamics subjected to different system parameters are described by the phase

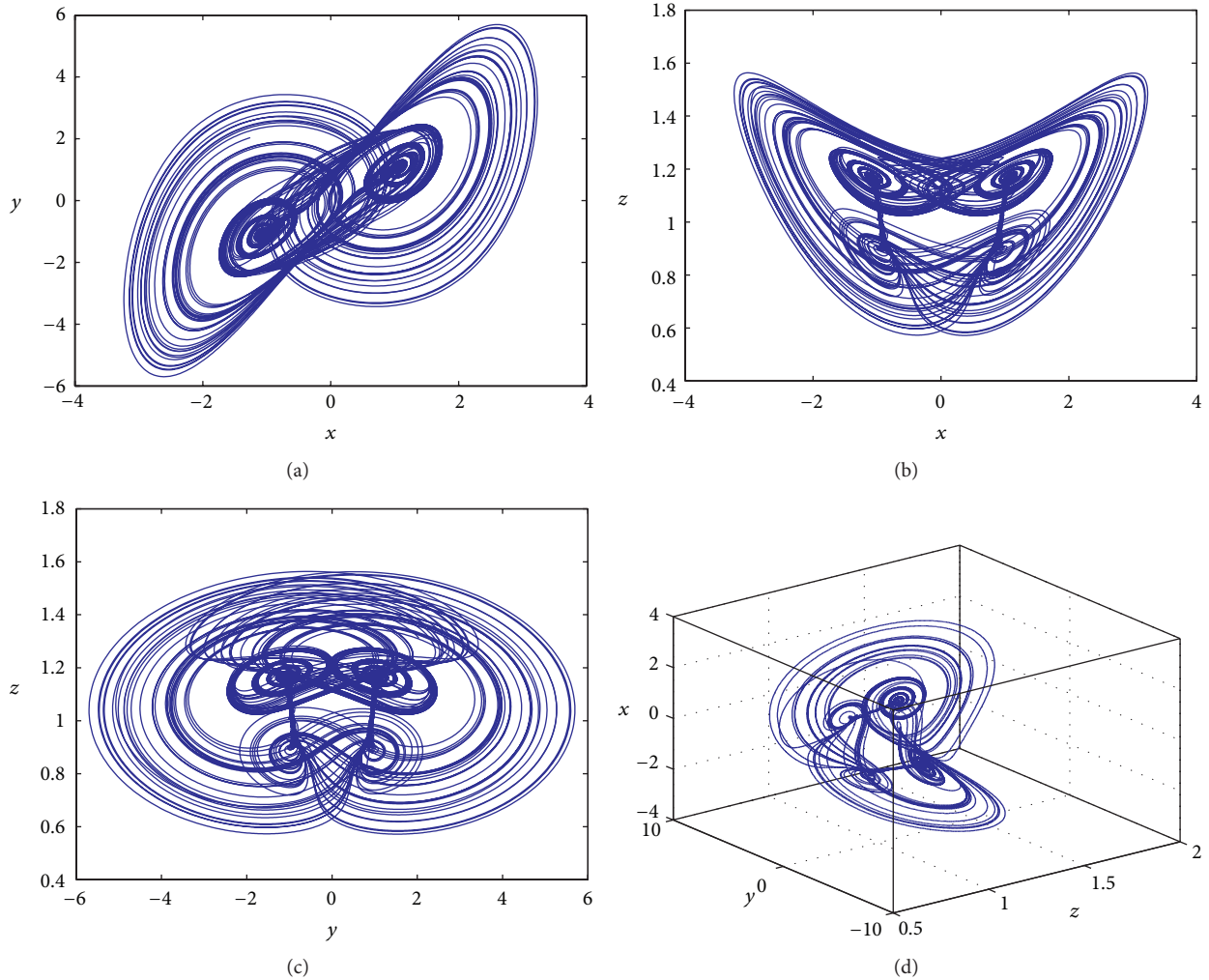


FIGURE 1: Phase portraits of the system (6) with $A = 0.2$, $\omega = 0.6$, $a = 10$, and $\gamma = 100$: (a) x - y plane; (b) x - z plane; (c) y - z plane; (d) x - y - z space.

portraits and the bifurcation diagrams that can be used to intuitively understand dynamics of the system (6). However, the phase portraits and the bifurcation diagrams cannot provide more information concerning frequency characteristics of a nonlinear system, and the power spectrum analysis is a useful tool to explore frequency characteristics.

As we all know, the power spectrum of periodic motion gives peaks at a primary frequency and its harmonics, and the power spectrum of quasiperiodic motion gives peaks at linear combinations of two or more irrationally related frequencies, and the power spectrum of chaotic motion gives continuous broadband components to the spectrum. When $A = 1$ and $\omega = 0.6$, the time series and power spectrum of variable x of the system (6) are shown in Figures 7(a) and 7(b), respectively. From Figure 7(a), it is obvious that the time series of variable x is periodic and the frequency f is approximately equal to $9/95 \approx 0.095$ Hz, which is in concordance with $\omega = 0.6$; namely, $f = \omega/2\pi \approx 0.095$ Hz. Moreover, the primary frequency 0.095 Hz and its higher harmonics 0.287 Hz, 0.475 Hz, 0.67 Hz, 0.86 Hz,

1.05 Hz, 1.24 Hz, and 1.43 Hz are shown in Figure 7(b) which further validate that the dynamics of the system (6) is periodic.

Chaotic signal, in contrast, has the properties of nonperiodicity, so the power spectrum is a continuous broadband. For the system (6), if $A = 0.2$ and $\omega = 0.6$, the time series and power spectrum of variable x are shown in Figures 8(a) and 8(b), respectively. Figure 8(a) shows random-like dynamics of variable x and the corresponding power spectrum shown in Figure 8(b) is continuous spectrum with noise-like background, which is one of the characteristics of chaotic signal. Through further analyzing of the power spectrum shown in Figure 8(b) and comparing it with the periodic power spectrum shown in Figure 7(b), it is easy to find that the primary frequency and its higher harmonics of the periodic signal generated from the system (6) at parameters $A = 1$ and $\omega = 0.6$ are still existing and act as the salient frequency components, but some new frequency components between the primary frequency and its higher harmonics are excited because of the change of the parameters of the driving signal

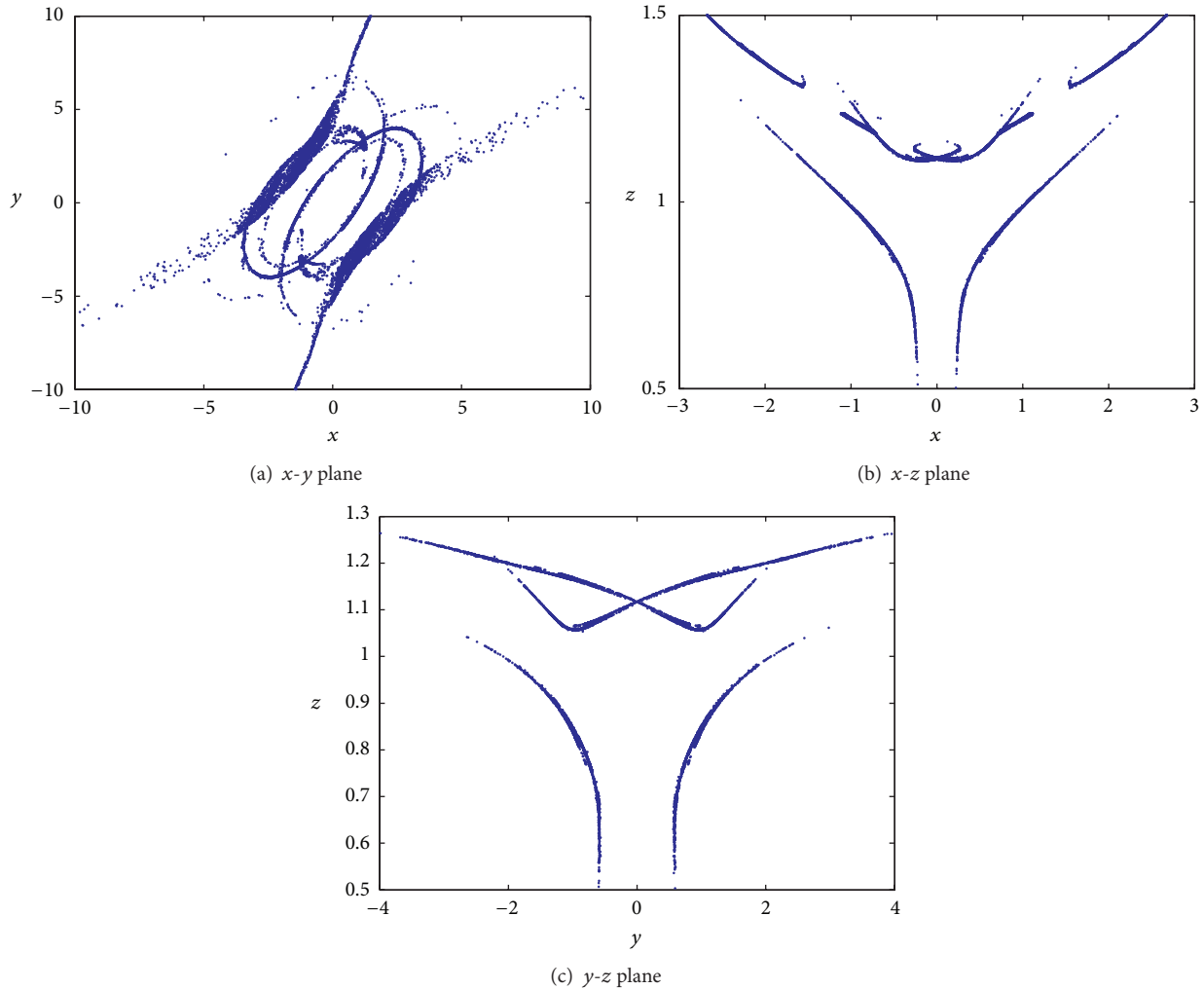


FIGURE 2: Poincaré sections: (a) $z = 0$; (b) $y = 0$; (c) $x = 0$.

\bar{v}_q . The excited frequency components are filled in other spectra of frequency, which forms a continuous frequency band. Because of its inadequate information of chaotic time series, richer frequency components are not wholly exhibited in Figure 8(b).

4. Circuit Implementation and Experimental Results

4.1. Experimental Circuit. A simpler implementation of a chaotic system can be achieved by an electronic circuit. With the help of the oscillators, the dynamics of many chaotic systems constructed by electronic circuit can be well demonstrated, which has been deeply researched in many chaotic systems. How to realize a chaotic experimental circuit has been investigated fully in [24, 25]. Here, the method is not introduced in details, but the schematic circuit and some necessary explanations are given.

The analog circuit for the nonautonomous system (6) is shown in Figure 9 and this circuit consists of three channels to conduct the integration of the three state variables x , y , and

z , respectively. The operational amplifiers LF347 (A1–A6) and associated circuitry perform the basic operations of addition, subtraction, and integration, and the values of resistors and capacitors are labeled in Figure 9. The nonlinear terms of the system (6) are implemented with two analogue multipliers AD633 (U1 and U2).

The periodic excitation signal $\bar{v}_q = A \sin(\omega t)$ is directly derived from a function generator YB1638. The input voltage frequency ω of the periodic excitation signal is 385 Hz and is fixed. It is necessary to point out that the angular frequency $\omega = 2\pi f$, where f is the frequency, can be directly and freely changed in the experimental environment.

Therefore, it is very convenient for us to change the value of parameters A and ω by adjusting the corresponding knobs in control panel. When we adjusted the amplitude A of the function generator YB1638, rich bifurcation phenomena emerged in the analogue oscilloscope YB4360.

4.2. Experimental Results. The bifurcation processes of chaos and periodic orbits can be obtained by changing the magnitude A of YB1638, and the corresponding strange chaotic

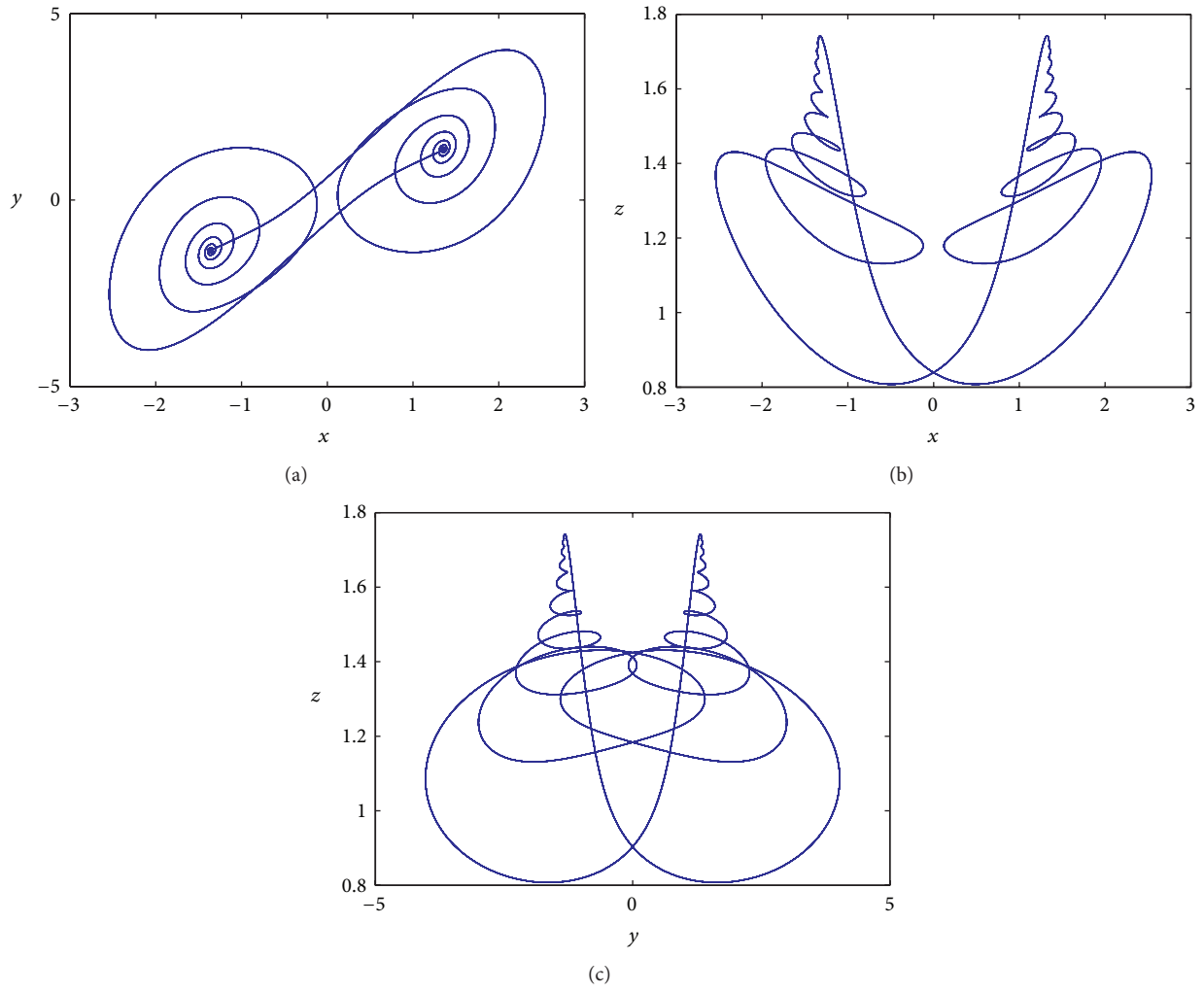


FIGURE 3: Phase portraits of the system (6) with $A = 1$, $\omega = 0.6$, $a = 10$, and $\gamma = 100$: (a) x - y plane; (b) x - z plane; (c) y - z plane.

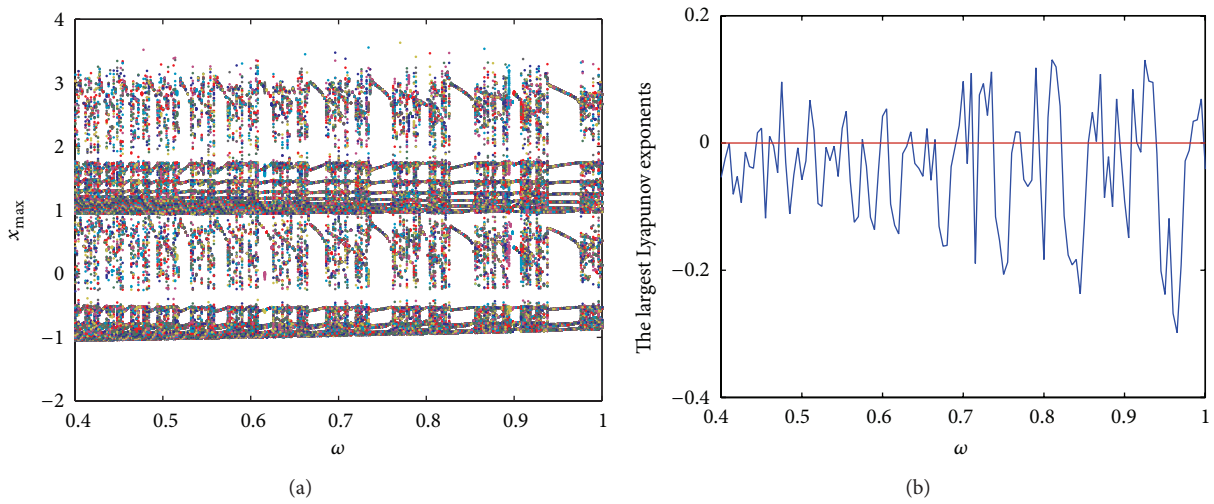


FIGURE 4: Dynamical behavior of the system (6) with ω in $[0.4, 1]$ and $A = 0.2$: (a) bifurcation diagram for increasing ω ; (b) the largest Lyapunov exponent versus ω .

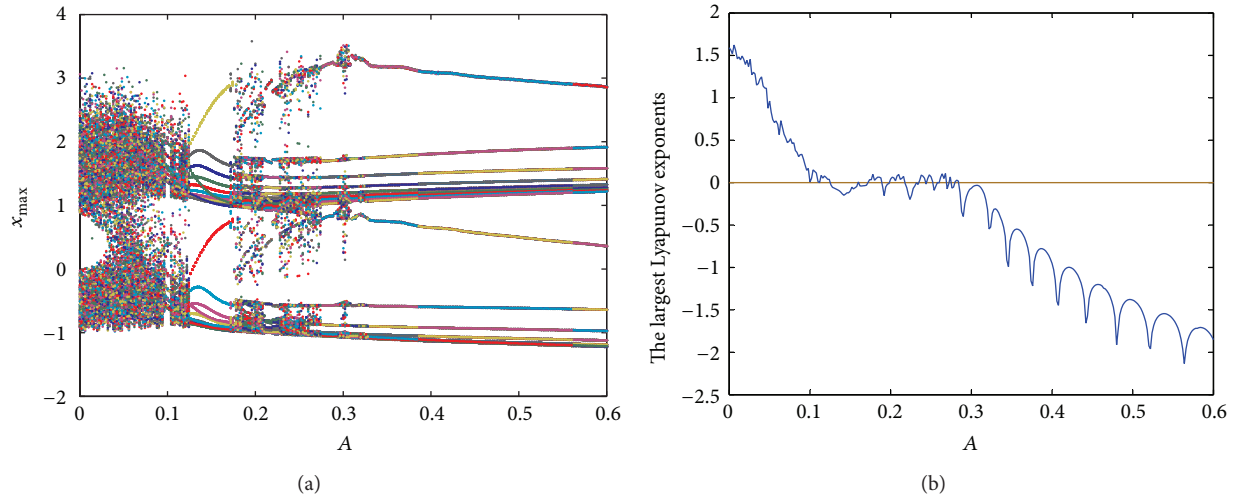


FIGURE 5: Dynamical behavior of the system (6) with A in $[0, 0.6]$ and $\omega = 0.6$: (a) bifurcation diagram for increasing A ; (b) the largest Lyapunov exponent versus A .

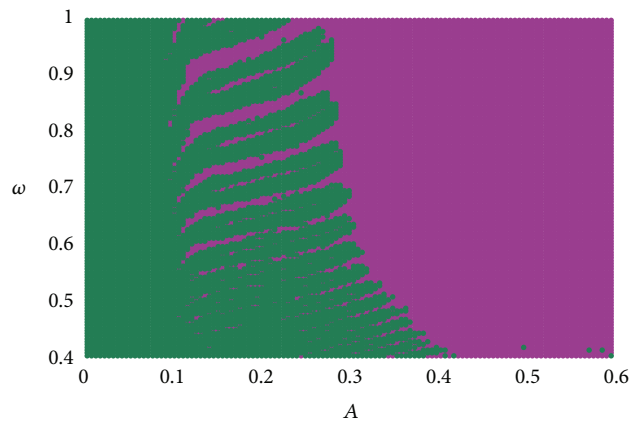


FIGURE 6: Two-dimensional dynamical behavior distribution on A - ω plane (colored figure online).

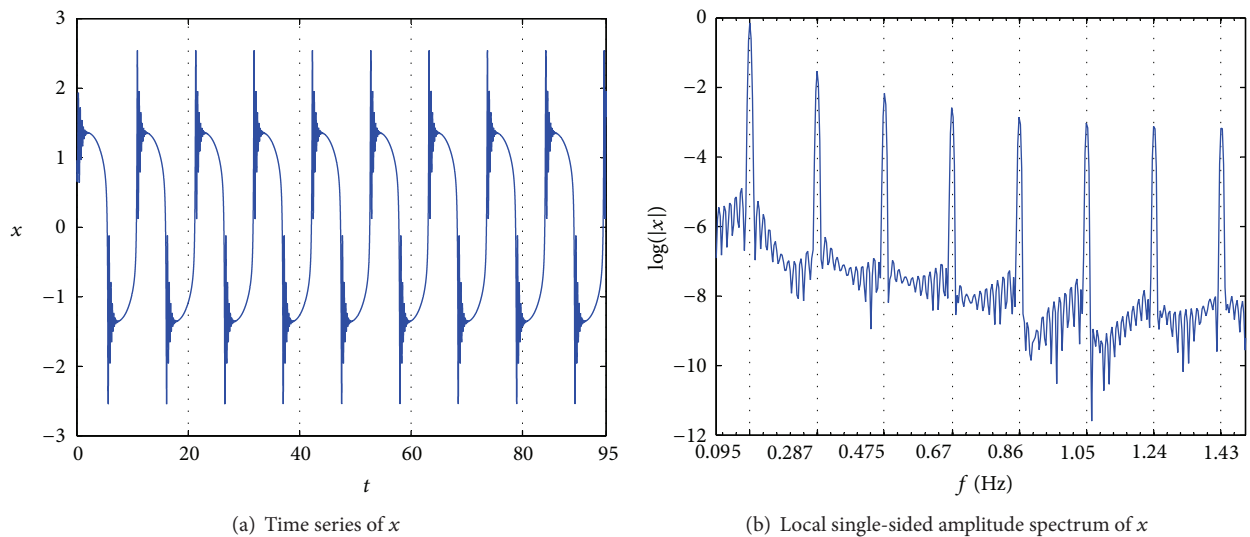


FIGURE 7: Time series and power spectrum of the system (6) with $A = 1$ and $\omega = 0.6$.

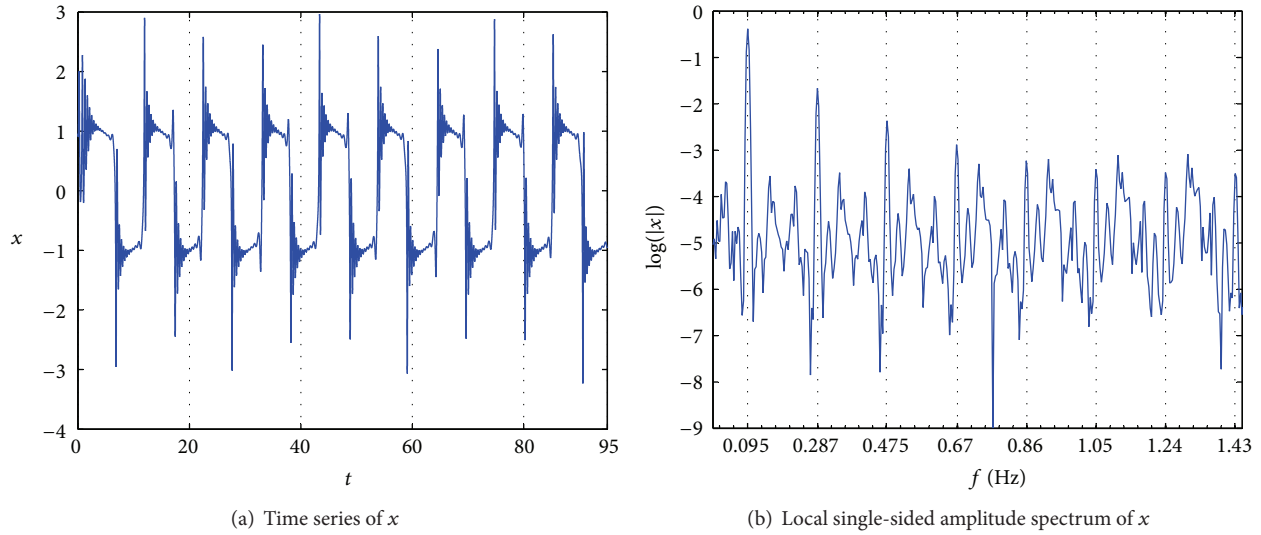


FIGURE 8: Time series and power spectrum of the system (6) with $A = 0.2$ and $\omega = 0.6$.

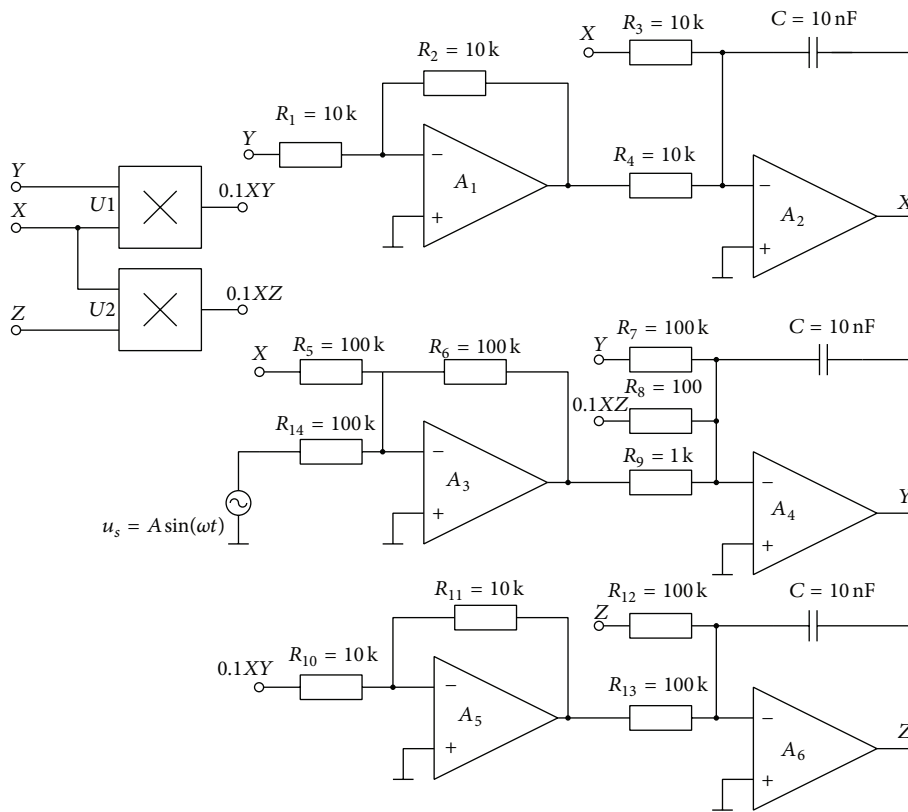


FIGURE 9: Circuit implementation of the system (6).

attractors and periodic orbits are shown in Figures 10(a)–10(c) and Figures 11(a)–11(c). As compared with Figures 1(a)–1(c) and Figures 3(a)–3(c), a good qualitative agreement between the numerical simulation and the experimental data was obtained. All results were recorded by YB4360.

But it should be pointed out that the obtained experimental results given above are not exactly the same as the numerical solutions in MATLAB even if the parameters were the same, since the chaos pattern is very sensitive to tiny changes in initial conditions (or during the evolution) and

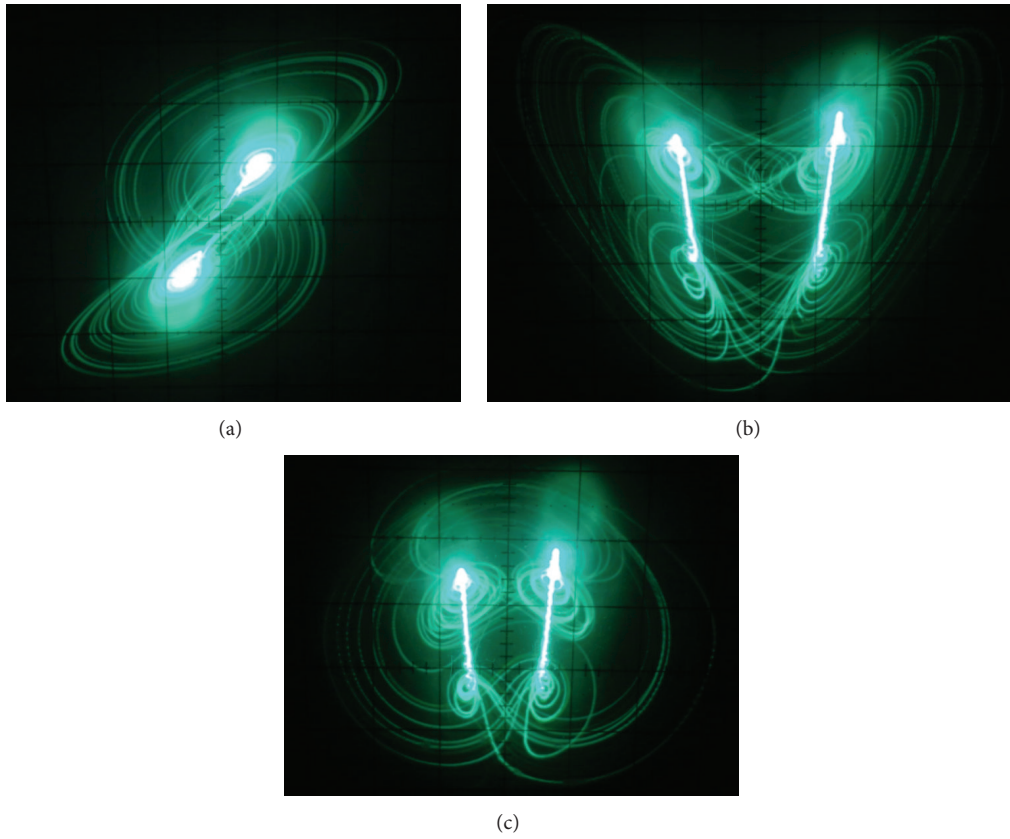


FIGURE 10: Chaotic motion shown in the phase portraits of the system (6) with $A = 0.8$ V and $f = 385$ Hz: (a) x - y plane; (b) x - z plane; (c) y - z plane.

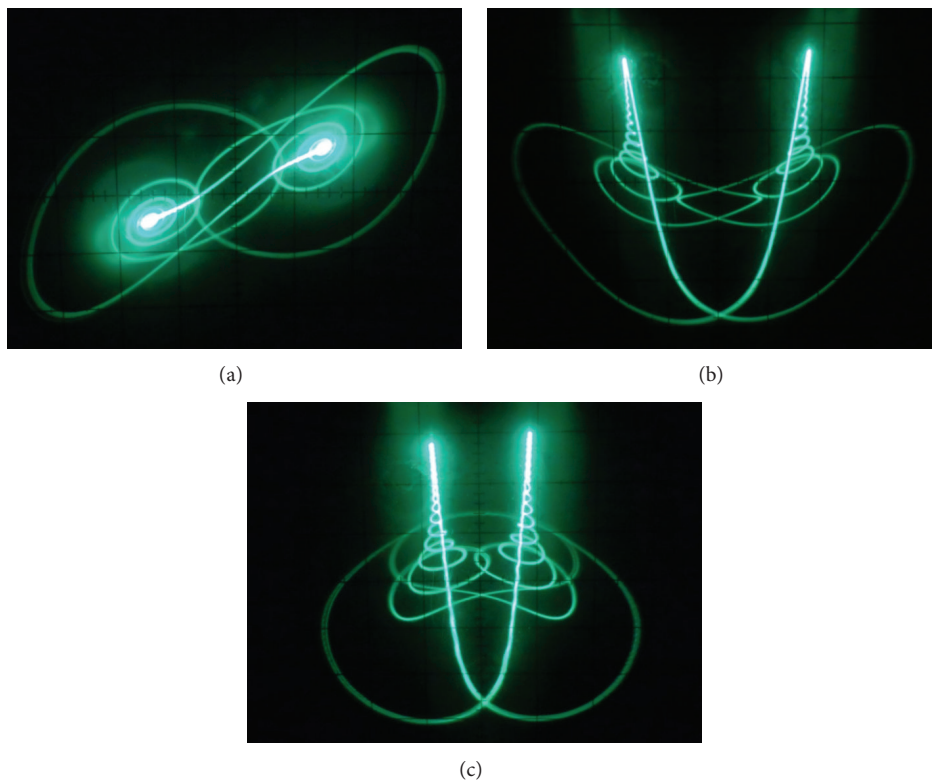


FIGURE 11: Multiperiodic orbit shown in the phase portraits of the system (6) with $A = 1.4$ V and $f = 385$ Hz: (a) x - y plane; (b) x - z plane; (c) y - z plane.

the modeling errors and environmental noise are unavoidable in hardware experiments.

5. Conclusions

In this paper, we put the emphasis on the investigation of a PMSM model with smooth air gap. By setting $\tilde{v}_q = A \sin(\omega t)$, a new nonlinear system having complex dynamical behavior was obtained. The resulting nonautonomous system with given parameters, which can be adjusted shrewdly and accurately by controlling the frequency and amplitude of the external periodic excitation, has shown significant characteristics that there exist a strange double-deck butterfly attractor and multiperiodic orbits. These phenomena have also been validated by the numerical simulations and an electronic circuit, and the experimental circuit showed that the phenomenon really exists in nature. Moreover, because the obtained chaotic attractor has a more complex topological structure that is not found in existing systems and is different from the existing four-wing chaotic attractors, the system (6) may have a good application value in the field of information technology such as secure communication and encryption. In the future we will conduct research on how to control the PMSM to escape from the chaotic behavior to protect the motors in the applications.

Conflict of Interests

The authors declare that they have no conflict of interests.

Acknowledgments

This work was supported in part by the Natural Science Foundation of China under Grant nos. 61174094 and 11202148, the Tianjin Natural Science Foundation under Grant no. 14JCYBJC18700, the Shandong Natural Science Foundation under Grant no. ZR2012FM034, the China/South Africa Research Cooperation Programme under Grant nos. 78673 and CS06-L02, and the South African National Research Foundation under Incentive Grant no. 81705.

References

- [1] D. Q. Wei, X. S. Luo, B. H. Wang, and J. Q. Fang, "Robust adaptive dynamic surface control of chaos in permanent magnet synchronous motor," *Physics Letters, Section A: General, Atomic and Solid State Physics*, vol. 363, no. 1-2, pp. 71-77, 2007.
- [2] C. Mademlis and V. G. Agelidis, "On considering magnetic saturation with maximum torque to current control in interior permanent magnet synchronous motor drives," *IEEE Transactions on Energy Conversion*, vol. 16, no. 3, pp. 246-252, 2001.
- [3] T. D. Batzel and K. Y. Lee, "Electric propulsion with sensorless permanent magnet synchronous motor: implementation and performance," *IEEE Transactions on Energy Conversion*, vol. 20, no. 3, pp. 575-583, 2005.
- [4] L. Jolly, M. A. Jabbar, and L. Qinghua, "Optimization of the constant power speed range of a saturated permanent-magnet synchronous motor," *IEEE Transactions on Industry Applications*, vol. 42, no. 4, pp. 1024-1030, 2006.
- [5] J. H. Lee, Y. J. Jang, and J. P. Hong, "Characteristic analysis of permanent magnet-assisted synchronous reluctance motor for high power application," *Journal of Applied Physics*, vol. 97, no. 10, Article ID 10Q503, 2005.
- [6] X. Zhang, X. Wang, J. Du, and R. Tang, "Amelioration of coreless permanent-magnet disk synchronous motor based on FEM: motor with wedge airgap," *Journal of Iron and Steel Research International*, vol. 13, no. 1, pp. 427-432, 2006.
- [7] L. Qi, X. Wang, J. Du, F. ZHAO, and R. TANG, "Magnetic field analysis of disk coreless permanent magnet synchronous motor based on thickness variation Halbach array," *Journal of Iron and Steel Research International*, vol. 13, no. 1, pp. 439-443, 2006.
- [8] S. Chi, Z. Zhang, and L. Xu, "Sliding-mode sensorless control of direct-drive PM synchronous motors for washing machine applications," *IEEE Transactions on Industry Applications*, vol. 45, no. 2, pp. 582-590, 2009.
- [9] N. Park, M. Jang, J. Lee, K. Hong, and J. Kim, "Performance improvement of a PMSM sensorless control algorithm using a stator resistance error compensator in the low speed region," *Journal of Power Electronics*, vol. 10, no. 5, pp. 485-490, 2010.
- [10] S. Chakraborty, E. Keller, A. Ray, and J. Mayer, "Detection and estimation of demagnetization faults in permanent magnet synchronous motors," *Electric Power Systems Research*, vol. 96, pp. 225-236, 2013.
- [11] Z. Li, J. B. Park, Y. H. Joo, B. Zhang, and G. Chen, "Bifurcations and chaos in a permanent-magnet synchronous motor," *IEEE Transactions on Circuits and Systems I: Fundamental Theory and Applications*, vol. 49, no. 3, pp. 383-387, 2002.
- [12] M. Zribi, A. Oteafy, and N. Smaoui, "Controlling chaos in the permanent magnet synchronous motor," *Chaos, Solitons & Fractals*, vol. 41, no. 3, pp. 1266-1276, 2009.
- [13] W. Xue, Y. L. Guo, and Z. Q. Chen, "Analysis of chaos and circuit implementation of a permanent magnet synchronous motor," *Acta Physica Sinica*, vol. 58, no. 12, pp. 8146-8151, 2009.
- [14] Z. J. Jing, C. Yu, and G. R. Chen, "Complex dynamics in a permanent-magnet synchronous motor model," *Chaos, Solitons and Fractals*, vol. 22, no. 4, pp. 831-848, 2004.
- [15] H. H. Choi, "Adaptive control of a chaotic permanent magnet synchronous motor," *Nonlinear Dynamics*, vol. 69, no. 3, pp. 1311-1322, 2012.
- [16] D. Wei, B. Zhang, and X. Luo, "Adaptive synchronization of chaos in permanent magnet synchronous motors based on passivity theory," *Chinese Physics B*, vol. 21, no. 3, Article ID 030504, 2012.
- [17] M. Ataei, A. Kiyomarsi, and B. Ghorbani, "Control of chaos in permanent magnet synchronous motor by using optimal Lyapunov exponents placement," *Physics Letters, Section A: General, Atomic and Solid State Physics*, vol. 374, no. 41, pp. 4226-4230, 2010.
- [18] K. Mischaikow and M. Mrozek, "Chaos in the Lorenz equations: a computer assisted proof. Part II: details," *Mathematics of Computation*, vol. 67, no. 223, pp. 1023-1046, 1998.
- [19] K. Mischaikow, M. Mrozek, and A. Szymczak, "Chaos in the Lorenz equations: a computer assisted proof Part III: classical parameter values," *Journal of Differential Equations*, vol. 169, no. 1, pp. 17-56, 2001.
- [20] M. Bask and R. Gençay, "Testing chaotic dynamics via Lyapunov exponents," *Physica D: Nonlinear Phenomena*, vol. 114, no. 1-2, pp. 1-2, 1998.
- [21] A. Algaba, F. Fernández-Sánchez, M. Merino, and A. J. Rodríguez-Luis, "Centers on center manifolds in the Lorenz,

- Chen and Lü systems,” *Communications in Nonlinear Science and Numerical Simulation*, vol. 19, no. 4, pp. 772–775, 2014.
- [22] S. Cang, G. Qi, and Z. Chen, “A four-wing hyper-chaotic attractor and transient chaos generated from a new 4-D quadratic autonomous system,” *Nonlinear Dynamics*, vol. 59, no. 3, pp. 515–527, 2010.
- [23] Z. H. Wang, G. Qi, Y. Sun, B. J. van Wyk, and M. A. van Wyk, “A new type of four-wing chaotic attractors in 3-D quadratic autonomous systems,” *Nonlinear Dynamics*, vol. 60, no. 3, pp. 443–457, 2010.
- [24] S. Cang, Z. Chen, and Z. Yuan, “Analysis and circuit implementation of a new four-dimensional non-autonomous hyperchaotic system,” *Acta Physica Sinica*, vol. 57, no. 3, pp. 1493–1501, 2008.
- [25] L. Liu, C. Liu, and Y. Zhang, “Theoretical analysis and circuit implementation of a novel complicated hyperchaotic system,” *Nonlinear Dynamics*, vol. 66, no. 4, pp. 707–715, 2011.